MODEL TYPE EFFECTS ON THE ESTIMATED SEISMIC RESPONSE OF A 20-STORY STEEL MOMENT RESISTING FRAME

Christos G. Lachanas[1] and Dimitrios Vamvatsikos[2]

Abstract: Finite element models of varying sophistication may be employed to determine a building's seismic response, with increasing complexity potentially offering higher fidelity at the cost of computational load. To account for this effect on the reliability of performance assessment, model-type uncertainty needs to be incorporated, as distinct to the uncertainty related to a given model's parameters. At present, only placeholder values are available in seismic guidelines. Instead, we attempt to accurately quantify them for a modern 20-story steel moment-resisting frame. Different types of 3D, 2D multi-bay, and 2D single-bay multi-degree-of-freedom models are investigated, together with their equivalent single-degree-of-freedom ones, to evaluate the model dependency of the response both within each broad model category, as well as among different categories. In conclusion, ensemble values are recommended for the uncertainty in each model category showing that for the perfectly-symmetric perimeter-frame P-Δ sensitive building under investigation, the uncertainty stemming from 3D versus 2D, or distributed versus lumped plasticity models is lower than the governing record-to-record variability.

CE Database subject headings: Earthquakes; Performance evaluation;

Author Keywords: seismic performance; model type uncertainty; pushover analysis; incremental dynamic analysis;

Introduction

The evaluation of the seismic performance of a structural system is associated with several uncertainty sources, which are either of aleatory or epistemic nature. Aleatory uncertainties are related with the inherent randomness of a natural phenomenon, such as the earthquake loading, and cannot be reduced. On the other hand, epistemic uncertainties are associated with the lack of knowledge or data and can be reduced through more experimental tests, such as the determination of material properties, or via more accurate models and methods of analysis (Der Kiureghian and Ditvelsen 2009; Wen et al. 2003). Nowadays, both the earthquake resistant design of new buildings and the assessment of the seismic performance of existing buildings are based on finite element models. Modern software enables the use of complex 3D models, elastic or inelastic, to assess the response of structures via linear or nonlinear analysis. However, when considering the seismic response of a building through nonlinear dynamic analysis, model complexity incurs significant computational cost. Especially in the context of strength reduction factor estimation (FEMA 2009), vulnerability assessment (D' Ayala et al. 2015) and regional loss estimation (Sousa et. al 2018; Sousa et al. 2016), the need to model

[1] PhD Student, Institute of Steel Structures, School of Civil Engineering, National Technical University of Athens, 9 Iroon Polytechneiou str., Zografou Campus, GR-15780 Athens, Greece (corresponding author). E-mail: lahanasch@central.ntua.gr, cglachanas@gmail.com
[2] Associate Professor, Institute of Steel Structures, School of Civil Engineering, National Technical University of Athens, 9 Iroon Polytechneiou str., Zografou Campus, GR-15780 Athens, Greece. E-mail: divamva@mail.ntua.gr

and analyze multiple archetype/index buildings favors the use of simpler 2D models, or even equivalent single degree of freedom (SDOF) ones. Similarly, different element modeling options may enhance or degrade accuracy in different ranges of response. For example, phenomenological lumped plasticity beam-column elements may capture better the near-collapse response, while distributed plasticity models can better capture the near-yield response (Haselton 2006). The end result is that potentially non-negligible modeling uncertainty is introduced.

Model uncertainty comprises two contributions (e.g., Bradley 2013). The first refers to model parameter uncertainty, i.e., the variability induced by uncertainties in the model parameters (strength, stiffness, mass, dimensions, etc.), and the second to model type uncertainty, or the variability that results from different modelling choices (e.g., 3D versus 2D model assumptions, type of finite element or damping model, the modeling or not of foundations and soil, etc.). Up until now, several studies (O'Reilly and Sullivan 2018; Kazantzi et al. 2014; Ibarra and Krawinkler 2011; Jalayer et al. 2010; Vamvatsikos and Fragiadakis 2010; Dolsek 2009; Liel et al. 2009; Kwon and Elnashai 2006; Wen et al. 2003; Porter et al. 2002; Yun et al. 2002) have investigated mainly model parameter uncertainty, finding small to moderate effects in most cases, especially for modern structures. Contrarily, on the subject of model type uncertainty, due to the practically unbounded range of options available, few comprehensive studies exist (e.g., Lignos et al. 2013; Chi et al. 1998). In general, uncertainty may introduce both bias and variance in our estimates of a building's performance. Bias is a systematic error that causes a deviation in the central value (mean or median) of our estimates. In other words, it represents a failure in capturing the true central value. Variance, on the other hand, concerns the added variability to an already uncertain response, akin to increased noise in the system. As long as the added variance is lower than the dispersion of the already-accounted-for governing source of variability (e.g., the natural aleatory variability due to records) its effect tends to disappear. At worst, if well quantified, it can be handled via standard probabilistic approaches present in any good framework (e.g., Cornell and Krawinkler 2000; or Cornell et al. 2002). For example, FEMA P-58 (FEMA 2012) and FEMA P695 (FEMA 2009) contain different proposals, based on expert opinion, for incorporating the added variability due to model quality. Bias instead is considered an important problem, as it cannot be handled reliably via statistical approaches: It necessitates the use of a bias correction factor for the central value of the distribution (mean or median), which generally cannot be estimated with sufficient reliability. Note that, in general, bias due to gross human errors cannot be accounted for. We are only discussing bias due to verifiable and acceptable engineering choices.

One of the few cases where such a bias correction has been employed is the spectral shape factor of FEMA P695 (FEMA 2009), which attempts to remove the bias due to scaling with an insufficient intensity measure. Otherwise, most guidelines tend to assume that bias does not exist, and models only incur additional variance. There is plenty of evidence, though, that this is not the case. For example, Chi et al. (1998) investigated the seismic response of a 17-story building damaged by the Northridge through different models. They examined the effect of neglecting characteristics such as three-dimensional torsion, secondary elements, and strength-stiffness degradation, showing that the choice of a model always comes with some bias.

On account of the above, while model type uncertainty is being widely recognized as a non-negligible uncertainty source, there are few (if any) numerical results on its actual impact on performance assessment. Aiming to provide such an outlook an initial attempt is made to quantify model type uncertainty for a plan-symmetric 20-story steel moment-resisting frame (SMRF). To this end, starting from the 3D frame model of the building, a gradual simplification of the model is undertaken: to 2D multi-bay frame (with or without basements), 2D single-bay frame and finally to SDOF model, as produced from the pushover analysis of the multi-degree-

of-freedom model (MDOF). All in all, 5 model categories are investigated, while in each MDOF model category there are alternative models with either lumped plasticity or distributed plasticity fiber section beam-column elements. Considerably more options are available in the literature, most notably by Elkady and Lignos (2015) on the influence of gravity frames, composite slabs, panel zones etc. In addition, one could incorporate the influence of soil-foundation-structure interaction, non-structural components, alternative damping models, or large displacement analysis (beyond just the inclusion of P-Delta effects). Instead, we chose to focus on more practice-oriented versions. The corresponding variance is thus certainly lacking in the breadth that it could attain with additional models investigated. Yet, it should still be representative of a wide range of practical options. Incremental Dynamic Analysis (IDA, Vamvatsikos and Cornell 2002; Vamvatsikos and Cornell 2004) is employed to assess the seismic response of each model. Our aim is to calculate the bias and variance stemming from the comparison between the performance of different models, in order to give engineers a sense of the level of safety and fidelity in their results, depending on the model type they use. It is important here to say that although SDOF models are considered to have low fidelity for the higher-mode influenced tall building under investigation, they are included for reasons of completeness.

Building Description

The building under investigation is the pre-Northridge SAC LA20, in the form originally modeled by Gupta and Krawinkler (1999). The building consists of 20 stories and 2 basements of the same regular plan. The basements are 3.66m (12ft) high, the first story 5.49m (18ft) and the ones above 3.96m (13ft). As shown in Fig. 1, there are 2 moment-resisting frames (MRFs) in each main direction consisting of 5 bays at 6.10m (20ft) in the X direction and 6 bays at 6.10m (20ft) in the Y direction. There is also an internal gravity frame connected to the external moment-resisting frames with beams 12.19m (40ft) in length. The MRF beams were designed according to low-ductility pre-Northridge standards, e.g., having no reduced beam section (RBS) connections. The corner columns are Hollow Square Sections (HSS), while the internal MRFs columns, the gravity columns, and the beams are wide flange sections (W). The structural steel quality is ASTM A36, with an expected yield strength of f_y = 339.22MPa (49.2ksi). Story masses, as proposed by Gupta and Krawinkler (1999), are 563.76t (38.63kipf·s^2/ft) at the roof of the ground floor, 551.06t (37.76 kipf·s^2/ft) at each typical floor and 584.63t (40.06kipf·s2/ft) at the roof of the 20 story. The total weight of the above-ground stories of the building comes to about 110,000kN and the damping ratio is 2%. The high aspect ratio (height over width) of the building results to a lateral deformation pattern that is a combination of shear and bending behaviour. Moreover, the aforementioned regularity in plan makes this building insensitive to torsional effects. Thus, lesser differences are expected when going from the 3D to the 2D model assumptions vis-à-vis plan-asymmetric buildings.

Analytical Modeling

A number of 3D/2D and equivalent 1D models have been generated. To distinguish them, a four-digit alphanumeric code is employed, with individual digits designating the following properties

1) M/S: To denote the number of degrees of freedom (MDOF or SDOF)
2) 3/2/1: to denote the dimensionality and size of the model, i.e., 3D or 2D multi-bay models (3 and 2, respectively) versus 2D one-bay models (1). This designation is kept even for SDOF equivalent models to better indicate which model the SDOF is representing.

3) B/G: To distinguish models incorporating the basements (B) from the ones stopping at the ground level (G).
4) 1/2/…/6: To distinguish different options in modeling beam-column elements, ranging from elastic to different choices in lumped plasticity or distributed plasticity nonlinear elements

Thus, for example, the M3B3 model is the 3D multi-bay distributed plasticity model with basements, M2G6 is the 2D multi-bay distributed plasticity model without basements, and S3B3, S2G6 are their corresponding equivalent SDOF models. Even for a single building configuration, these four variables make for a wide model space that cannot be explored fully. We did not examine all the combinations, trying e.g. to have 1:1 correspondence between the 3D and 2D models developed. Instead we tried to explore the parameter space by diverse structural models that still represent feasible engineering designs. In the following, the different model types adopted are discussed in detail.

3D with Basements (*M3Bx*)

The first model category refers to the full 3D frame model of the building (Fig. 2(a)). This is formed in the OpenSees open-source analysis platform using beam-column elements for both MRF and gravity frame members. Centerline dimensions were employed without modeling the panel zones. This is a modeling choice that could make a difference for older steel frames with flexible panels but this is not the case for the case at hand (Foutch and Yun 2002; Gupta and Krawinkler 1999). Both basement stories are included in the model in order to properly incorporate the flexibility of the ground floor columns. Masses were placed at each diaphragm and gravity loads were assigned to the columns according to their tributary areas. 2% Rayleigh damping was assumed at the first and fourth mode of vibration. Alternative, non-Rayleigh damping models are also possible (Chopra and McKenna 2016; Hall 2006), but not considered herein. For all models, P-Δ effects were taken into account through a first-order treatment. Due to plan symmetry, the first two modes of vibration are translational in X and Y and of nearly the same period, with the X direction being slightly more flexible due to having one less bay.

For the first model of this category (M3B1), lumped plasticity elements were employed for the MRF and gravity frame columns of the first story and all the MRF beams, while all gravity columns and all MRF columns above the first floor were modeled as elastic. For the inelastic elements, stiffness was modeled using the (elastic hardening with kinematic hysteresis) Steel01 material (OpenSees 2006). Post yield hardening was set at 1%, while for the gravity frame beams a reduction of hinge stiffness (*E*) and plastic moment capacity (M_{pl}) at 25% of their initial values was assumed (Foutch and Yun 2002), since they are shear-only connections. In the second model of this category (M3B2) both columns and beams were modeled as lumped plasticity elements using a similar approach to M3B1. For the corner columns of the MRF, no reduction for biaxial moment interaction was assumed by using independent point-hinge springs in each axis. The third model (M3B3) employs distributed plasticity fiber section elements. The Hardening material (OpenSees 2006), using an elastic-hardening backbone with 0.3% hardening and kinematic hysteresis was employed, whilst each member section was divided into ten fibers along height and width and into two fibers along thickness. The members were modeled as force-based elements, while five integration points along each member were assumed using Gauss-Lobatto integration (Scott 2011), which places integration points at the member ends, where the maximum bending moments and strains at MRFs members are expected. Gravity frame beams were modeled as lumped plasticity elements similarly to the aforementioned 3D models because of their small contribution to the total seismic response and their nearly pinned connection to the columns. For all models, diaphragms were implemented via a kinematic constraint. Despite the use of a distributed plasticity fiber element for the beams of model M3B3, this does not introduce any parasitic

axial forces in the beams due to their symmetric behavior under positive versus negative bending moments. Composite action between the beam and the slab at the plastic hinge region (Elkady and Lignos 2014) was disregarded, thus assuming no shear studs in this area (per typical design practice) and an adequate gap between the slab and the column flange.

2D no Basements (*M2Gx*)

As discussed, the first model simplification from 3D model to 2D model refers to the 2D multi-bay frame model. Only the X-axis MRF is modeled (Fig. 2(b)) being the more flexible. In all cases, a 2D analytical model was developed in OpenSees without basements. P-Δ effects were included using a first-order treatment of geometric nonlinearity. Additionally, a leaning column was added to account for gravity frame mass and stiffness. 2% Rayleigh damping at the first two modes of vibration was assumed. The first model (M2G1), similarly to the previous 3D category, employs lumped plasticity elements for all beams and the ground floor columns while elastic elements were employed for the columns above the first floor. For the rotational springs, elastic hardening behavior with 1% hardening ratio was assumed using the Pinching4 material (OpenSees 2006). Similarly, in the second model (M2G2) both beams and columns were modeled as lumped plasticity members.

Models M2G3 to M2G5 employ lumped plasticity elements with an Ibarra and Krawinkler (2005) material law as this was modified by Lignos and Krawinkler (2011), for the idealization of the rotational springs at the member ends. The rotational hinge parameters were determined according to the expressions proposed by Lignos and Krawinkler (2011) for "other than RBS" connections. In particular, the effective yield strength M_y is assumed equal to $1.17M_{pl}$ due to overstrength, whereas the post-yield strength ratio is $M_c/M_y = 1.10$ and the residual strength is $M_r = 0.40M_y$. The yield rotation for double curvature bending was assumed to be $\theta_y = M_yl/(6EI)$ where l is the length of the member, while the pre-capping θ_p and the post-capping θ_{pc} plastic rotation were computed as per Lignos and Krawinkler (2011) depending on the section's height d. Due to the fact that the proposed relationships refer to W sections, the corner columns (HSS) were taken as equivalent W sections in terms of section area and major axis moment of inertia for quantifying the parameters. The ultimate rotation capacity θ_u was estimated to be 0.05 to 0.06rad for "other-than RBS" beams, but as mentioned by Lignos and Krawinkler (2011) it can be up to three times as large. For M2G3, the model employs only the rotations θ_y and θ_p as mentioned above, while the effective yield-strength was taken as $M_y =1.00M_{pl}$ rather than $1.17M_{pl}$. The hardening ratio was assumed 1% and the capping negative slope equal to the 10% of the initial section stiffness. For M2G4 and M2G5 all the recommendations of Lignos and Krawinkler (2011) were followed using $\theta_u = 0.06$ for the former and $\theta_u = 0.18$ for the latter. Finally, for M2G6 distributed plasticity force-based elements were employed for both beams and columns.

2D with Basements (*M2Bx*)

The second 2D multi-bay frame category represents a direct 2D analogue of the M3Bx 3D models. In particular, the M2Bx model (Fig. 2(c)) comprises one MRF in the X direction of the corresponding 3D model (M3Bx). Here, similarly to the 2D without basements models, there is a leaning column for the gravity frames and a first-order treatment of P-Δ effects. In direct correspondence to the 3D models, M2B1 employs elastic columns for the 2nd story and above, while the ground floor columns and all beams use phenomenological lumped plasticity elements; in M2B2 all beams and columns were modeled as lumped plasticity elements, whereas in M2B3 all members were modeled as distributed plasticity fiber-section elements. One additional model without a 3D analogue, namely M2B4, was also employed using lumped plasticity hinges at the member ends, each represented by a single fiber section and appropriate

plastic hinge length. This offers a compromise between M2B2 and M2B3 offering interaction of axial force and bending moment at a relatively low computational cost.

2D One Bay with Basements (M1Bx)

Offering further reduction in complexity a 2D single-bay frame model is considered (Fig. 2 (d)). There is a long history of such models, stemming back at least to Luco et al. (2003). Herein, a single 20ft (6.10m) bay model is employed, incorporating both basements, a leaning column, and P-Δ effects. Only lumped plasticity elements are employed, as axial-moment interaction cannot properly be accounted for, due to the lumping of multiple columns into one. A key issue to mention for this category is the column area adjustment that is required to capture the actual bending stiffness of the building. While this model type can reliably capture the shear stiffness of the building, due to its lower width it needs to be adjusted to properly represent its bending stiffness, otherwise it fails to accurately capture even the first-mode period of a tall structure. On account of the above, the moments of inertia of the beam and the two columns representing each story are computed as:

$$I_{beam} = \sum_{i=1}^{n_b} I_{beam,i} \tag{1}$$

$$I_{column} = \frac{1}{2}\sum_{i=1}^{n_c} I_{column,i} \tag{2}$$

where n_b is the number of beams and n_c the number of columns per story of the multi-bay frame, while $I_{beam,i}$ and $I_{column,i}$ are the bending moments of inertia of the given story's i-th beam and column, respectively. These are sufficient to account for beam shear behavior. To also capture the system bending behavior, the section area A of the columns needs to be increased to A_O in each story. This can be easily done by considering the composite section of the N columns of the multi-bay model versus the two columns of its one-bay version and matching their moments of inertia around the neutral axis:

$$2A_O\left(\frac{L}{2}\right)^2 = \sum_{i=1}^{N}(A_i x_i{}^2) \Leftrightarrow A_O = 2\sum_{i=1}^{N}\left[A_i\left(\frac{x_i}{L}\right)^2\right] \tag{3}$$

where L is the bay length, A_i the section area of column i, and x_i the horizontal distance of column i from the gravity center of the N columns along the side of the multi-bay 2D model. If A_H is the corner column area and A_W the internal column area of the MRF (Fig. 3), then Eq. (3) becomes:

$$A_O = 2[2A_H(2.5^2) + 2A_W(1.5^2) + 2A_W(0.5^2)] = 4(6.25A_H + 2.5A_W) \tag{4}$$

This adjustment is the main advantage of this model type in comparison with fishbone models (Luco et al. 2003, Nakashima et al. 2002). The latter are of similar complexity, yet by having only a single column per story they cannot easily display the proper bending stiffness without some careful calibration. In general, for buildings with aspect ratio (height over width) less than 2.5–3.0 this adjustment may be neglected (Luco et al. 2003). Similarly to the 2D no basement models (M2Gx), M1B1–M1B5 are direct analogues of M2G1–M2G5 but with basements included. M1B1 employs lumped plasticity elements for all beams and the ground floor columns, while the rest of the columns are elastic. In M1B2 all columns and beams were modeled as lumped plasticity elements, whereas M1B3–M1B5 used lumped plasticity

members using the Ibarra and Krawinkler model (2005) as modified by Lignos and Krawinkler (2011) for rotational spring idealization at the member ends.

Equivalent SDOF systems (Sxxx)

For each one of the 18 aforementioned MDOF models the equivalent SDOF model is produced through nonlinear static (pushover) analysis. Specifically, a 1D nonlinear spring with multilinear backbone curve was employed in OpenSees (Pinching 4 material). The spring's force deformation (F^*-δ^*) backbone curve and period (T^*) are determined as (Fajfar 2000):

$$m^* = \frac{aM}{\Gamma} \tag{5}$$

$$F^* = \frac{V_{base}}{\Gamma} \tag{6}$$

$$\delta^* = \frac{\delta_{roof}}{\Gamma} \tag{7}$$

$$T^* = 2\pi \sqrt{\frac{m^* \delta_y^*}{F_y^*}} \tag{8}$$

where a is the percentage of the total mass M participating in the MDOF's first-mode response, m^* is SDOF mass, whereas Γ is the first-mode participation factor to transform from MDOF to equivalent SDOF response parameters and vice-versa. V_{base}-δ_{roof} represent points of the MDOF capacity curve, while F_y^*-δ_y^* are the yielding points of the F^*-δ^* fitted curve. Fitting was done using a four-segment piecewise-linear approximation as illustrated in Fig. 4 for the M3B2 to S3B2 conversion. Finally pushover analysis results were used to transform δ^* to δ_{roof} (Eq. (7)) and the maximum interstory drift ratio (θ_{max}) of the building.

Performance Assessment

Fig. 5 illustrates the capacity curves for the MDOF models. Pushover analysis employed a second-order lateral-load pattern for the 3D models in order to include higher mode shapes:

$$F_i = F_b \frac{w_i z_i^2}{\sum(w_i z_i^2)} \tag{9}$$

where F_b is the total lateral load and w_i, z_i are the i-th story weight and height. All other categories employed a first-mode pattern. As illustrated, all model types capture the elastic behavior of the building (elastic branch). Still, the 2D models where the full expressions of Lignos and Krawinkler (2011) were employed have notably higher strength due to the 1.17 overstrength factor of the effective yield strength M_y, having at the same time lower ductility because of the restricted ultimate rotational capacity of the members. Models with elastic column elements have a shallower negative stiffness segment as expected, while the fiber models are somewhat distinguished from the lumped plasticity ones by showing lower strength in 3D models, potentially due to biaxial effects. This difference is eliminated in 2D models. In general, though, most of the differences are found in the post-peak region, i.e. for roof drifts greater than 1.5-2.0%. This is despite the differences in the models adopted for beams and

columns and can be attributed to the significance of the P-Δ effects that govern the behavior of the structure. Shorter buildings with less P-Δ influence will generally better bring out the differences among the various element models.

IDA is employed to determine the seismic response of the models. As Intensity Measure (IM), we use the 5% damped first-mode spectral acceleration $S_a(T_1,5\%)$, in X direction (arbitrary component). In addition, the geometric mean of both horizontal components, $S_{agm}(T_1,5\%)$, as well as the average spectral acceleration $AvgS_a$ were employed at the level of summarizing the final results. $AvgS_a$ is defined as the geometric mean of spectral ordinates from both horizontal components (Kazantzi and Vamvatsikos 2015; Eads et al. 2015; Tsantaki and Adam 2013; Bianchini et al. 2009; Vamvatsikos and Cornell 2005a; Cordova et al. 2000):

$$AvgS_a = \left[\prod_{i=1}^{n} S_a(T_{Ri})\right]^{1/n} \tag{10}$$

T_{Ri} are the reference periods, herein chosen according to Kazantzi and Vamvatsikos (2015) to be $[T_2, \min[(T_2+T_1)/2, 1.5 \cdot T_2], T_1, 1.5 \cdot T_1, 2 \cdot T_1]$. Although the periods among different models and different horizontal axes within a model do not show large differences, to ensure a common IM, the X-direction periods of the M3B2 were used to define S_a and $AvgS_a$ for all models. In general, $AvgS_a$ is more efficient and sufficient as an IM but $S_a(T_1,5\%)$ is still widely used (FEMA 2012) so we compute model type uncertainty for both of them. As Engineering Demand Parameter (EDP), the maximum interstory drift ratio in X direction (θ_{max}) and the peak floor acceleration in X direction (*PFA*) were employed, as indicative of structural and non-structural damages. Y direction values are disregarded as they cannot be captured by the 2D or 1D models. Thirty ordinary (no long duration, no pulse-like characteristics) ground motion records (PEER 2005; Chiou et al. 2008) were used from five earthquake events; they are characterized by firm soil (types C/D per NEHRP classification) with moment magnitude ranging from 6.53-6.93. For 3D models both horizontal components were employed, while only one arbitrary component was assigned to 2D and SDOF models. Representative individual IDA curves and the corresponding fractiles appear in Fig. 6 for model M3B2.

Comparison Between Models

Table 1 presents the results of the modal and the pushover analysis for the 36 models under investigation. The periods of the 1st, 2nd and 4th mode for the M3Bx models, the first two modes for 2D models and T^* for SDOF models are reported. The 4th mode of the M3Bx models is translational in X direction and corresponds to the 2nd mode of the 2D multi-bay models (M2Gx, M2Bx). In addition, the maximum base shear V_{max} from pushover analysis and the maximum F^* of SDOF fitted F^*-δ^* curve are presented. Finally, the computational time required for the pushover, t_{po}, is offered as an indication of the complexity of the model. The pushover analysis was performed on a laptop with an Intel Core i7 6500U @2.50GHz central processing unit using identical analysis setting (number of steps, convergence, tolerance etc.) for all models. For SDOF models no time is recorded, as it is essentially the same as the t_{po} of the corresponding MDOF model.

As shown in Table 1, there are non-negligible differences in computational time between 3D and 2D models as also among distributed plasticity and lumped plasticity models. It makes little sense to offer computational times for a single record dynamic analysis, because there is considerable record-to-record dependence. For the entire suite of 30 records, the M3B3 model IDA's computational time is about 55 hours, for the M3B2 about 25 hours, and about 20 hours for M3B1. For 2D models, the computational time ranges within 2–4 hours, whereas for SDOFs it is less than 0.10 hours.

In processing the results of different models, one needs to account for the within-model or intra-model variability, typically due to record-to-record aleatory randomness, and the between-model or inter-model variability that stems from the fundamental differences between different model types. In all practical assessment situations, an engineer will only have access to a single model, which he/she can potentially subject to a set of ground motion records and determine the intra-model variability. On the other hand, having no comprehensive suite of alternative models, he/she will not be able to assess the level of bias in his/her single model. This is why the intra-model term can be thought of as the primary variance of the assessment results, while the inter-model term is essentially a measure of the distribution of bias in a classic bias-variance decomposition (Hastie et al. 2009) of the overall inference problem.

Incorporating the bias and variance terms into one's results requires making a choice. One may opt to discard the decomposition of model type uncertainty into its bias and variance components and instead treat both as variance. This is the so-called first-order assumption typically adopted in Performance Based Earthquake Engineering (FEMA 2012; FEMA 2009; Cornell et al. 2002), whereby all sources of non-modelled uncertainty are assumed not to introduce bias, leaving the central value of response distributions unchanged, offering only additional variability. Thus, the total variability theorem (or law of total variance) (Weiss 2005) can be employed to combine the intra-model variability (original variance) with the inter-model variability (original bias) of n models to estimate the total, typically assuming an underlying lognormal distribution for both:

$$\beta_{total}^2 = \beta_{intra}^2 + \beta_{inter}^2$$

$$\beta_{intra}^2 = \frac{1}{n}\sum_{j=1}^{n}\beta_{j,intra}^2 \qquad (11)$$

$$\beta_{inter}^2 = \frac{1}{n-1}\sum_{j=1}^{n}(\ln\overline{x_{50}} - \ln x_{50}^j)^2$$

where x_{50}^j is the median EDP given IM or IM given EDP for model j, and $\overline{x_{50}}$ is the mean of all x_{50}^j.

Alternatively, one may choose to handle bias separately from variance. Then, rather than assuming that one's model is perfectly unbiased, a bias correction factor is employed instead of fixing any deviations in the central (mean or median) value of the distribution. This approach obviously comes with heavy consequences as a baseline "accurate" model is required, as well as its response for seismic motion. Obviously, this can be the case only in academic studies, perhaps such as the present one, although in all frankness, none of the 18 + 18 models employed can come close to the accuracy of running actual shake table tests of the structure. Thus, employing this approach without some concrete data (e.g. from testing or validated numerical models) to back the choice of a bias correction factor is obviously haphazard akin to the use of a "fudge" factor. The advantage is clearly the one of reduced dispersion, as, by offering an accurate bias correction, one needs only employ the β_{intra} of the model (or at worst the average β_{intra}) rather than the β_{total} of Eq. (11).

Therefore, although only the first-order assumption is the recommended option for comparison due to the aforementioned issues, we shall discuss both options: The first one for general use and the second for understanding the contributions of both sources of uncertainty. To this effect, we show results for the relative bias in the median IM given EDP vis-à-vis the baseline model considered to be most accurate in each group of models delineated in the

following. Specifically, we only show results for θ_{max}, dividing the [0, 10%] range into $j = 1,…,200$ discrete values. Then, the relative bias for the i-th model and the j-th θ_{max} value is:

$$bias_{i,j} = \frac{S_{\alpha 50\%}(T_1, 5\%) \mid \theta_{max}^{j} \text{ for model } i}{S_{\alpha 50\%}(T_1, 5\%) \mid \theta_{max}^{j} \text{ for baseline model}} - 1 \qquad (12)$$

Comparison within Each Model Category

The comparison among models starts within each broad model category, where the relative bias remains low; thus, only the first-order assumption is fully applicable and only variance results are shown per category Eq. (11). Record-to-record variability β_{intra} is similar for the n models of each category and practically the same as their mean, which remains at about 0.40 for the majority of θ_{max} values. As illustrated in Fig. 7(b,d,f,h), record-to-record variability has a dominant effect on the total MDOF dispersions. On the other hand, model-to-model dispersion within the M3Bx and M2Bx categories is less than 0.05 for $\theta_{max} \leq 4\%$. Higher model-to-model dispersion appears in M2Gx and M1Bx models, especially for drift ratios of 2–4%, due to the aforementioned overstrength of some encountered in cases, where the full expressions of Lignos and Krawinkler (2011) were employed. In contrast, as shown in Fig. 8(b), the two components of variability have a similar contribution to the total dispersion of SDOFs, especially, for drift ratios higher than 1.5% where the large differences due to fitting the capacity curve inadvertently increase the inter-model variability.

Comparison among Different Model Categories

Between models of different categories, bias can be considerable. Thus, results for both of the two bias-variance treatments are shown. The variance for the first-order assumption, β_{total}^{2}, is calculated from Eq. (11), similarly to the comparison within each model category. For the second option, bias was computed by Eq. (12) for the same 200 θ_{max} values linearly spread within 0–10%. Furthermore, as summarized measures of bias over multiple models and the entire range of response, we employ the average absolute bias *avgbias$_j$* for each j-th θ_{max} value for the n models of each set, and its mean, *avgball*, over the 160 discrete θ_{max} values among 0% and 8%:

$$avgbias_j = \frac{1}{n}\sum_{i=1}^{n}\left|bias_{i,j}\right| \qquad (13)$$

$$avgball = \frac{1}{160}\sum_{j=1}^{160}\left|avgbias_j\right| \qquad (14)$$

The comparison was made both between models with similar element types and between more widely varied model sets. The baseline ("perfect") model for each set is the 3D one. Among models with lumped plasticity elements and models with distributed plasticity elements, the first were assumed more reliable, because they perform better near collapse. In addition, results of comparison both with and without the inclusion of SDOF models are presented due to their low fidelity for a high-rise structure.

Fig. 9 shows the comparison results between the models where distributed plasticity fiber section elements were employed versus the corresponding SDOFs, with M3B3 assumed as the baseline model. As illustrated, record-to-record variance has higher contribution to the total dispersion than the inter-model variability that ranges from 0.02–0.11 for θ_{max} up to 4%. At the same time, relative bias (Fig. 9(b)) varies within 0–0.10 for the MDOF models. As expected, SDOFs introduce higher bias and dispersion when they were included into the calculation. For

low θ_{max} ratios (<3%) SDOFs shows negative bias ratios due to the "hardening" behavior of the MDOFs: The latter show on average lower deformations than what the equal displacement rule would imply, or equivalently higher IM values for the same deformation compared to the SDOFs. The SDOFs also fail to capture the significant P-Δ effects that dominate the response of the building. By assuming three limit states (LS) at the specific θ_{max} thresholds of 0.75%, 2%, 4%, which approximate the "immediate occupancy", "life safety" and "near collapse" LS, the *avgbias* was calculated equal to 0.02, 0.14, and 0.05 respectively, whereas *avgball* = 0.14. When excluding the SDOFs from the calculations we get *avgbias* = 0.03, 0.08, 0.05 at the three LS and *avgball* = 0.05, all becoming clearly lower.

Likewise, Fig. 10 illustrates the results for a set of 2D models. Specifically, the set includes all the 2D models from M2Gx, M2Bx and M1Bx model categories except for the models where elastic elements were employed for the columns. The M2B4 was assumed as the baseline model for the relative bias calculation. From the IDA curves, the M_y overstrength of the models, where the full expressions of Lignos and Krawinkler (2011) were employed, becomes apparent for $\theta_{max} > 2.50\%$. Thus, those models show high "bias" (>0.2) at high θ_{max} ratios, while this fact also affects the inter-model dispersion for this set at the same drift ratios. Here, at the three LS, *avgbias* = 0.03, 0.02, 0.17, while *avgball* = 0.09. Note that the selection of the baseline model naturally colors our results. Had we chosen as baseline the models based on the expressions of Lignos and Krawinkler (2011), e.g. M2G4, all others would become associated with bias. Hence such values should be taken as indicative of the differences among models, rather than an actual judgement on their merits.

Fig. 11 presents the comparison among all the models that were employed for the purposes of this study, where the 3D lumped plasticity model (M3B2) was assumed as the baseline model. In general, the 2D models show lower strength than the 3D models (negative bias) except for those where the full expressions of Lignos and Krawinkler (2011) were employed. Moreover, the IDA curves of the SDOFs that were produced from those models match better with the IDA curves of the MDOFs due to the lower ductility of those MDOFs because of the restricted ultimate rotational capacity of the members. As illustrated in Fig. 11(d) and Fig. 11(e) there is notable difference in the inter-model variance when SDOFs are included. Specifically, model-to-model dispersion until the "near collapse" LS varies within 0.04–0.12 without SDOFs and within 0.08–0.18 when taking them into account. At the three LSs considered, we got *avgbias* = 0.08, 0.19, 0.15 and *avgball* = 0.15 with SDOFs, whilst *avgbias* = 0.09, 0.10, 0.14 and *avgball* = 0.13 when these were excluded from the calculations.

Now, we turn to the mean (average) response (μ) of each model type. Fig. 12(a) illustrates the average of the median IDA curves within each model category, whereas the relative bias of the mean response to the baseline 3D category (M3Bx), as it was calculated via Eq. (12), is captured in Fig. 12(b). In general, 2D models show lower strength than the 3D ones with relative bias within 0–0.18. Yet, M2Gx and M1Bx models differs from the M2Bx models for θ_{max} within 2–4% due to the overstrength of the models where the full expressions of Lignos and Krawinkler (2011) were employed. On the other hand, SDOFs fail to capture both the hardening behavior of the MDOFs at drift values within 2–4% and the significant P-Δ effects of the 20-story building. This does not preclude the use of different fitting approaches or pushover-based methods that can better capture the MDOF response (Vamvatsikos and Cornell 2005b; Chopra and Goel 2002), but the results obtained with the general N2 method (Fajfar 2000) are certainly indicative of the difficulty in getting reliable outputs out of an SDOF system for a higher-mode influenced building.

Fig. 13(a) depicts the ratio of the record-to-record dispersion (β_{intra}) of each broad model category over the β_{intra} of M3Bx models. As illustrated, 2D model categories show in general similar record-to-record variability with 3D models, while SDOFs show remarkably lower record-to-record variability for drift values up to 5% due to the model's low sophistication

level (single spring model). Furthermore, Fig. 13(b) shows the bias of mean SDOFs response over the corresponding MDOFs mean response for each model category. The results confirm the aforementioned differences between SDOF and MDOF median IDA curves. In addition, the bias for M2Gx and M1Bx categories is higher than M3Bx and M2Bx due to the restricted ductility of some models (M2G3, M1B3) that affects the SDOFs backbones and consequently the IDA curves of those equivalent SDOF models as also captured in Fig. 8(a).

Provisional Recommendations

A final recommended total variance for each model category was calculated based on the first-order assumption and the total variability theorem (Eq. (11)). For the most sophisticated model category, M3Bx, which is assumed to be the baseline, β_{total} can only come from the results of the group of 3D models, as captured in Fig. 7(b). Then, for the next category in terms of model complexity and fidelity (2D full bay frame) Eq. (11) can be expanded as:

$$\beta_{totalFM2Gx}^2 = \text{mean}(\beta_{totalM3Bx}^2, \beta_{totalM2Gx}^2) + [\text{std}(\mu_{M3Bx}, \mu_{M2Gx})]^2 \tag{15}$$

$$\beta_{totalFM2Bx}^2 = \text{mean}(\beta_{totalM3Bx}^2, \beta_{totalM2Bx}^2) + [\text{std}(\mu_{M3Bx}, \mu_{M2Bx})]^2 \tag{16}$$

where mean($x_1, x_2, \ldots, x_N$) and std($x_1, x_2, \ldots, x_N$) denote taking the mean and the standard deviation, respectively, of their arguments $x_1, x_2, \ldots, x_N$; μ_X and β_{totalX} are the mean and total dispersion, respectively, of IM given the EDP response of category X. Considering M2Gx and M2Bx as a single 2D multi-bay frame category leads to:

$$\beta_{totalF2DFULL}^2 = \text{mean}(\beta_{totalM3Bx}^2, \beta_{totalM2Gx}^2, \beta_{totalM2Bx}^2) + [\text{std}(\mu_{M3Bx}, \mu_{M2Gx}, \mu_{M2Bx})]^2 \tag{17}$$

Moreover, for the M1Bx the final total dispersion was calculated as:

$$\beta_{totalFM1Bx}^2 = \text{mean}(\beta_{totalM3Bx}^2, \beta_{totalM2Gx}^2, \beta_{totalM2Bx}^2, \beta_{totalM1Bx}^2) + [\text{std}(\mu_{M3Bx}, \mu_{M2Gx}, \mu_{M2Bx}, \mu_{M1Bx})]^2 \tag{18}$$

Finally, for the SDOFs keeping in mind the dominant bias effect that is present and makes the first-order assumption quite questionable, the total variance is:

$$\beta_{totalFSxxx}^2 = \text{mean}(\beta_{totalM3Bx}^2, \beta_{totalM2Gx}^2, \beta_{totalM2Bx}^2, \beta_{totalM1Bx}^2, \beta_{totalSxxx}^2) + [\text{std}(\mu_{M3Bx}, \mu_{M2Gx}, \mu_{M2Bx}, \mu_{M1Bx}, \mu_{Sxxx})]^2 \tag{19}$$

Fig. 14(a), shows the total variances as these were computed from Eq. (15)–(19) with θ_{max} as EDP. The final total dispersion ranges from 0.36 to 0.43 both for the 3D models and the 2D models, whereas being lower for the SDOFs due to the lower intra-model dispersion and consequently lower β_{total} for those models Fig. 8(b), Fig. 13(a). By changing the EDP to *PFA* in the X direction for MDOF categories (as a *PFA* estimate cannot be easily rendered by SDOFs), Fig. 14(b) illustrates the remarkably higher total variance that was calculated, namely 0.68–0.78, with 3D models coming a bit higher compared to the 2D ones.

Taking the geometric mean of both the horizontal components, $S_{agm}(T_1, 5\%)$, as IM in Fig. 15, 3D models show higher dispersions than the 2D ones, whereas both for 3D and 2D categories lower dispersions were obtained when *PFA* was employed as EDP vis-à-vis the arbitrary component, $S_a(T_1, 5\%)$, results. Similar results were taken for θ_{max} when the average

spectral acceleration, $AvgS_a$, was employed as IM (Fig. 16), while lowered values were also found for PFA, in line with the findings of Kazantzi and Vamvatsikos (2015).

Conclusions

The model type effects on the estimated seismic response are presented for a symmetric regular 20-story steel moment-resisting frame. During analysis, the significant computational cost that is associated with the use of 3D models was confirmed, as well as, the differences in computational time between the models with distributed plasticity elements and those with lumped plasticity elements due to difficulties in convergence for the former. The use of lumped plasticity elements with fiber-end-sections strikes an obvious compromise between the two.

In addition, the models where the full expressions of Lignos and Krawinkler (2011) were employed, show significant overstrength vis-à-vis just employing an average steel yield strength, especially for the post-elastic response. The total dispersion within each MDOF model category varies within 0.33–0.42, the record-to-record variability within 0.33–0.41 and the model-to-model dispersion among 0.01–0.15 for interstory drift ratios up to 4%.
Relative bias among the MDOF models for the elastic, the near-(nominal)-yield and the near-collapse response ranges from -0.20 to 0.20. This low bias for the latter two cases is mainly due to the significant P-Δ effects for this tall building, which dominate the response at high displacements, thus dwarfing the contribution of modeling details. This would not be the case if, for example, a plan-asymmetric or lower height (e.g. 6-story) building was investigated. Considerable relative bias also appears for SDOFs as their fidelity is quite low for a high-rise.

As a final proposal, the total dispersion of the MDOFs varies within 0.33–0.45 when the maximum interstory drift ratio is employed as EDP, being about the same for all the spectral acceleration IMs used and practically equaling the record-to-record variability. When the peak floor acceleration was employed as EDP, the final total dispersion ranges from 0.60–0.78 for all the MDOF categories when the first-mode spectral acceleration (arbitrary or geomean) is the IM, while lower values of 0.55-0.68 apply for the average spectral acceleration. Note that current literature recommends additional uncertainties due to model parameters of 0.05–0.15, which implies that, if the two contributions are combined in a square-root-sum-of-squares fashion, record-to-record variability will dominate over all sources of uncertainty.

Furthermore, the aforementioned results denote that for a regular building without significant torsion effects there is no big difference among 3D and 2D models. In other words, the building under investigation is an ideal building for separating the response in X direction and the response in Y direction. This fact is supported by the symmetry of the SMRFs, where only the corner columns operate in the two main direction simultaneously during the seismic response. Nevertheless, it is suspected that the model type effects may rise in importance for irregular buildings, shorter buildings or for buildings with lateral-load resisting systems that cannot easily redistribute lateral forces.

Data Availability Statement

Some or all data, models, or code that support the findings of this study are available from the corresponding author upon reasonable request:
- All structural analysis data generated in the study.

Acknowledgements

References

Bianchini, M., Diotallevi, P., Baker, J. W. (2009). "Prediction of Inelastic Structural Response Using an Average of Spectral Accelerations". *The 10th International Conference on Structural Safety and Reliability (ICOSSAR09)*, Osaka, Japan.

Bradley, B. A. (2013). "A critical examination of seismic response uncertainty analysis in earthquake engineering." *Earthquake Engineering and Structural Dynamic*, 42(11), 1717–1729.

Chi, W., El-Tawil, S., Deierlein, G. G., and Abel, J. F. (1998). "Inelastic Analyses of a 17 Story Framed Building Damaged During Northridge." *Engineering Structures*, 20(4), 481–495.

Chiou, B., Darragh, R., Gregor, N., Silva, W. (2008). "NGA Project Strong-Motion Database." *Earthquake Spectra*, 24(1), 23–44.

Chopra, A. K., McKenna, F. (2016). "Modeling viscous damping in nonlinear response history analysis of buildings for earthquake excitation." *Earthquake Engineering and Structural Dynamics*, 45, 193–211.

Chopra, A. K., Goel, R. K. (2002). "A modal pushover analysis procedure for estimating seismic demands for buildings." *Earthquake Engineering and Structural Dynamics,* 31 (3), 561–582.

Cordova, P. P., Deierlein, G. G., Mehanny, S. S., Cornell, C. A. (2000). "Development of a two parameter seismic intensity measure and probabilistic assessment procedure." *The Second U.S.-Japan Workshop on Performance-Based Earthquake Engineering Methodology for Reinforced Concrete Building Structures*, Sapporo, Hokkaido, 187–206.

Cornell C. A., Jalayer, F., Hamburger, R. O., Foutch, D. A. (2002). "The probabilistic basis for the 2000 SAC/FEMA steel moment frame guidelines." *ASCE Journal of Structural Engineering*, 128(4), 526–533.

Cornell, C. A., Krawinkler, H. (2000). Progress and challenges in seismic performance assessment. *PEER Center News*, 3(2), 1–4.

D'Ayala, D., Meslem, A., Vamvatsikos., D., Porter., K., Rossetto., T., Silva., V. (2015). *Guidelines for analytical vulnerability assessment of low/mid-rise buildings – Methodology*. Pavia, Italy: Vulnerability Global Component Project. DOI 10.13117/GEM.VULN-MOD.TR2014.12

Der Kiureghian, A., Ditvelsen, O. (2009). "Aleatory or epistemic? Does it matter?" *Structural Safety*, 31(2), 105–112.

Dolsek, M. (2009). "Incremental dynamic analysis with consideration of modelling uncertainties." *Earthquake Engineering and Structural Dynamics*, 38(6), 805–825.

Eads, L., Miranda, E., Lignos, D., G. (2015). "Average spectral acceleration as an intensity measure for collapse risk assessment." *Earthquake Engineering and Structural Dynamics*, 44, 2057–73.

Elkady, A., Lignos, D. G. (2015). "Effect of gravity framing on the overstrength and collapse capacity of steel frame buildings with perimeter special moment frames." *Earthquake Engineering and Structural Dynamics*, 44, 1289–1307.

Elkady, A., Lignos, D. G. (2014). "Modeling of the composite action in fully restrained beam-to-column connections: implications in the seismic design and collapse capacity of steel special moment frames." *Earthquake Engineering and Structural Dynamics*, 43, 1935–1954.

FEMA. (2012). *Seismic Performance Assessment of Buildings*. FEMA P-58, prepared by the Applied Technology Council for the Federal Emergency Management Agency, Washington, D.C.

FEMA. (2009). *Quantification of Building Seismic Performance Factors*. FEMA P-695, prepared by Applied Technology Council for Federal Emergency Management Agency, Washington, D.C.

FEMA. (2000). *Recommended Seismic Evaluation and Upgrade Criteria for Existing Welded Steel Moment-Frame Buildings*. FEMA-351, prepared by the SAC Joint Venture for the Federal Emergency Management Agency, Washington, DC.

Foutch, D. A., Yun, S. Y. (2002). "Modeling of steel moment frames for seismic loads." *Journal of Constructional Steel Research*, 58, 529–564.

Gupta, A., Krawinkler, H. (1999), *Seismic demands for performance evaluation of steel moment resisting frame structures.* John A. Blume Earthquake Engineering Center Report No. 132, Department of Civil and Environmental Engineering, Stanford University, California.

Hall, J. F. (2006). "Problems encountered from the use (or misuse) of Rayleigh damping." *Earthquake Engineering and Structural Dynamics*, 35, 525-545. doi:10.1002/eqe.541

Haselton, C. B. (2006). *Assessing Seismic Collapse Safety of Modern Reinforced Concrete Moment*

Frame Buildings. Ph.D. Dissertation, Department of Civil and Environmental Engineering, Stanford University.

Hastie, T., Tibshirani, R., Friedman, J. (2009). *The Elements of Statistical Learning* (2nd edition). Springer-Verlag. http://statweb.stanford.edu/~tibs/ElemStatLearn/ (Feb. 04, 2020).

Ibarra, L., and Krawinkler, H. (2011). "Variance of collapse capacity of SDOF systems under earthquake excitations." *Earthquake Engineering and Structural Dynamics*, 40, 1299–1314.

Ibarra, L. F., and Krawinkler, H. (2005). *Global collapse of frame structures under seismic excitations*. Report. No. TB 152, The John A. Blume Earthquake Engineering Center, Stanford University, Stanford, CA.

Jalayer, F., Iervolino, I., and Manfredi, G. (2010). "Structural modeling uncertainties and their influence on seismic assessment of existing RC structures." *Structural Safety*, 32(3), 220–228.

Kazantzi, A. K., Vamvatsikos, D. (2015). "Intensity measure selection for vulnerability studies of building classes." *Earthquake Engineering and Structural Dynamics*, 44(15), 2677–2694.

Kazantzi, A. K., Vamvatsikos, D., Lignos, D. G. (2014). "Seismic performance of a steel moment-resisting frame subject to strength and ductility uncertainty." *Engineering Structures*, 78, 69–77.

Kwon, O. S., and Elnashai, A. (2006). "The effect of material and ground motion uncertainty on the seismic vulnerability curves of RC structure." *Engineering Structures*, 28(2), 289–303.

Liel, A. B., Haselton, C. B., Deierlein, G. G., Baker, J. W. (2009). "Incorporating modeling uncertainties in the assessment of seismic collapse risk of buildings." *Structural Safety*, 31(2), 197–211.

Lignos, D. G., Hikino, T., Matsuoka, Y., Nakashima, M. (2013). "Collapse Assessment of Steel Moment Frames Based on E-Defense Full-Scale Shake Table Collapse Tests." *ASCE Journal of. Structural. Engineering*, 139 (1), 120–132.

Lignos, D. G., and Krawinkler, H. (2011). "Deterioration Modeling of Steel Components in Support of Collapse Prediction of Steel Moment Frames under Earthquake Loading." *ASCE Journal of Structural Engineering*, 137(11), 1291–1302.

Luco, N., Mori, Y., Funahashi, Y., Cornell, C. A., and Nakashima, M. (2003). "Evaluation of predictors of nonlinear seismic demands using "fishbone" models of SMRF buildings." *Earthquake Engineering and Structural Dynamics*, 32(14), 2267–2288.

Nakashima, M., Ogawa, K., and Inoue, K. (2002). "Generic Frame model for Simulation of Earthquake Responses of Steel Moment Frames." *Earthquake Engineering and Structural Dynamics*, 31(3), 671–692.

OpenSees (2006). *Open System for Earthquake Engineering Simulation*. Pacific Earthquake Engineering Research Center, University of California, Berkeley, Available at http://opensees.berkeley.edu/. (Feb. 04, 2020).

O'Reilly, G.J., Sullivan, T.J. (2018) "Quantification of modelling uncertainty in existing Italian RC frames." *Earthquake Engineering and Structural Dynamics*, 47, 1054- 1074.

PEER (2005). PEER NGA Database. Pacific Earthquake Engineering Research Center, Berkeley, CA, http://peer.berkeley.edu/nga/. (Feb. 04, 2020).

Porter, K. A., Beck, J. L., Shaikhutdinov, R. V. (2002). "Sensitivity of building loss estimates to major uncertain variables." *Earthquake Spectra*, 18(4), 719–743.

Scott, M. H. (2011). "Numerical integration options for force-based beam-column element in OpenSees." Oregon State University, Corvallis.

Sousa, L., Silva, V., Marques, M., Crowley., H. (2018). "On the treatment of uncertainty in seismic vulnerability and portfolio risk assessment." *Earthquake Engineering and Structural Dynamics*, 47, 87–104.

Sousa, L., Silva, V., Marques, M., and Crowley, H. (2016). "On the treatment of uncertainties in the development of fragility functions for earthquake loss estimation of building portfolios." *Earthquake Engineering and Structural Dynamics*, 45, 1955–1976.

Tsantaki, S., Adam, C. (2013). "Collapse capacity spectra based on an improved intensity measure." *The 4th ECCOMAS Thematic Conference on Computational Methods in Structural Dynamics and Earthquake Engineering (COMPDYN 2013)*, Kos, Greece.

Vamvatsikos, D., Fragiadakis, M. (2010). "Incremental Dynamic Analysis estimating seismic performance uncertainty and sensitivity." *Earthquake Engineering and Structural Dynamics*, 39(2), 141–163.

Vamvatsikos, D., Cornell, C. A. (2005a). "Developing efficient scalar and vector intensity measures for

IDA capacity estimation by incorporating elastic spectral shape information." *Earthquake Engineering and Structural Dynamics*, 34(13): 1573–1600.

Vamvatsikos, D., Cornell, C. A. (2005b). "Direct estimation of the seismic demand and capacity of MDOF systems through Incremental Dynamic Analysis of an SDOF Approximation." *ASCE Journal of Structural Engineering*, 131(4): 589–599.

Vamvatsikos, D., Cornell, C. A. (2004). "Applied Incremental Dynamic Analysis." *Earthquake Spectra*, 20(2), 523–553.

Vamvatsikos, D., Cornell, C. A. (2002). "Incremental Dynamic Analysis." *Earthquake Engineering and Structural Dynamics*, 31(3), 491–514.

Vamvatsikos D., Institute of Steel Structures, National Technical University of Athens, Greece http://users.ntua.gr/divamva/software.html (Feb. 04, 2020).

Weiss, N. A. (2005). *A Course in Probability*. Addison–Wesley.

Wen, Y. K., Ellingwood, B. R., Veneziano, D., and Bracci, J. (2003). *Uncertainty Modeling in Earthquake Engineering*. MAE Center Project FD-2 Report, Mid-America Earthquake Engineering Center.

Yun, S., Hamburger, R., Cornell, C., and Foutch, D. (2002). "Seismic Performance Evaluation for Steel Moment Frames." *ASCE Journal of Structural Engineering*, 4(534), 534–545.

Figures

(a)

(b)
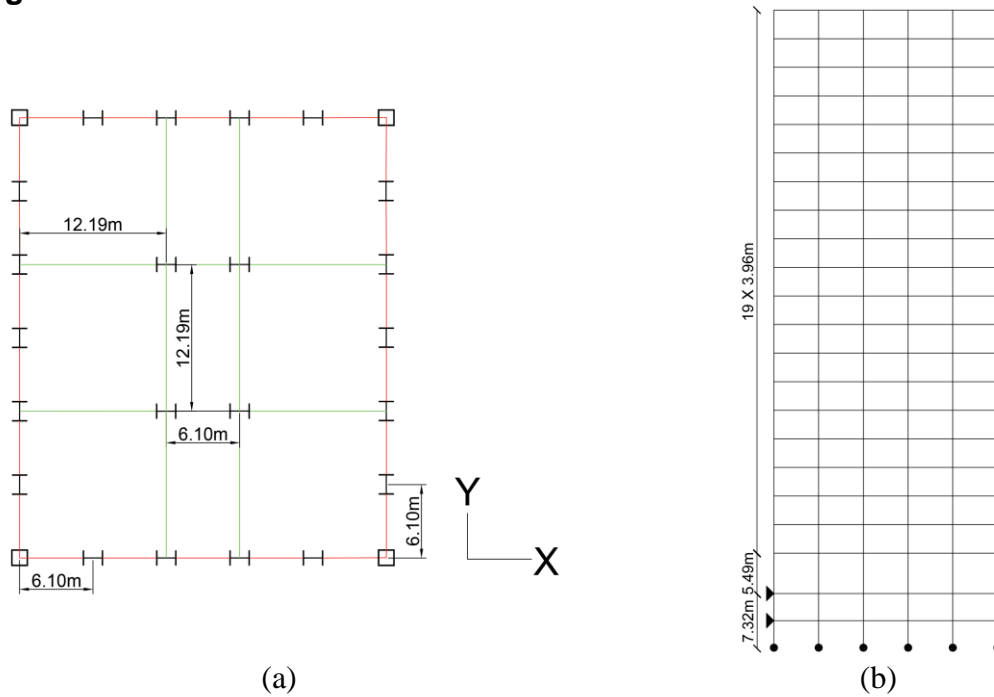
Fig. 1. (a) Plan of the building. (b) MRF in X direction.

(a) (b) (c) (d) (e)
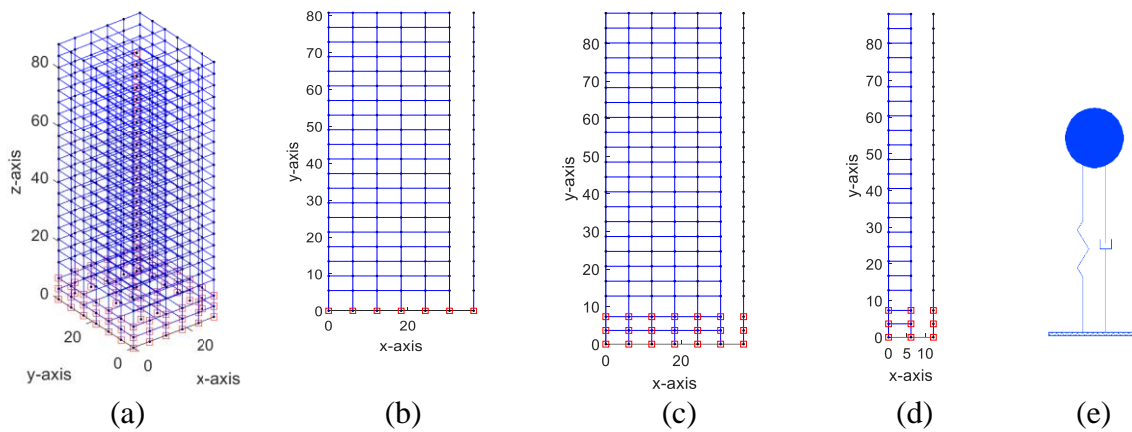
Fig. 2. Building models (red circles denote the ground level and the basements): (a) M3Bx model (the central node at each floor is indicated in red). (b) M2Gx model. (c) M2Bx model. (d) M1Bx model. (e) Sxxx model.
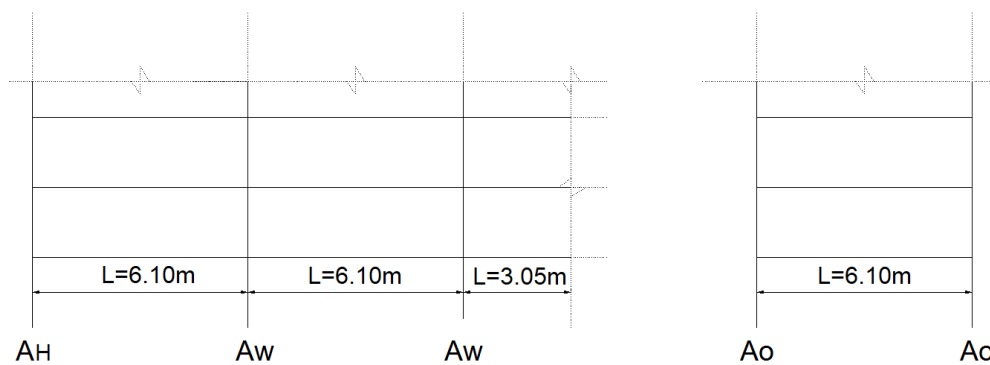
Fig. 3. View of the left half of the MRF in the X direction (left) and of the single-bay frame model (right).
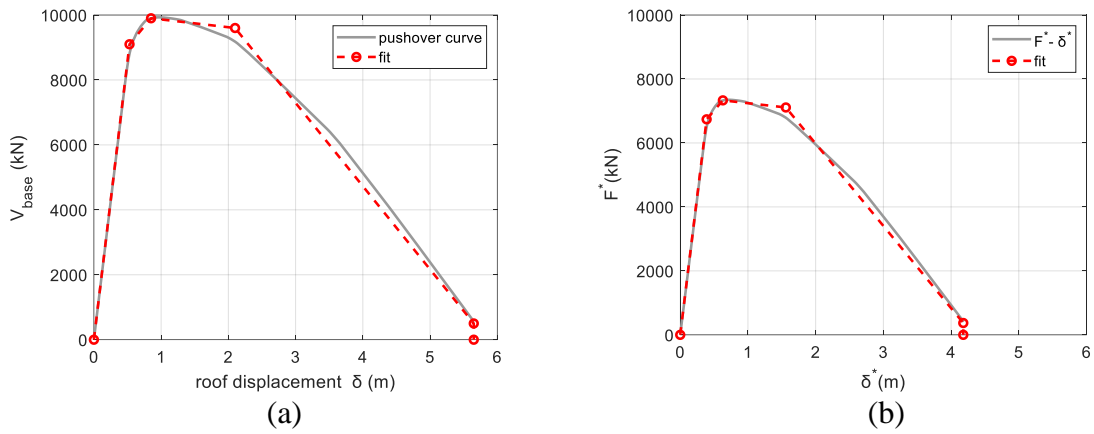
Fig. 4. Backbone fitting to generate an Sxxx model: (a) M3B2 Pushover curve. (b) S3B2 F^*-δ^* curve.
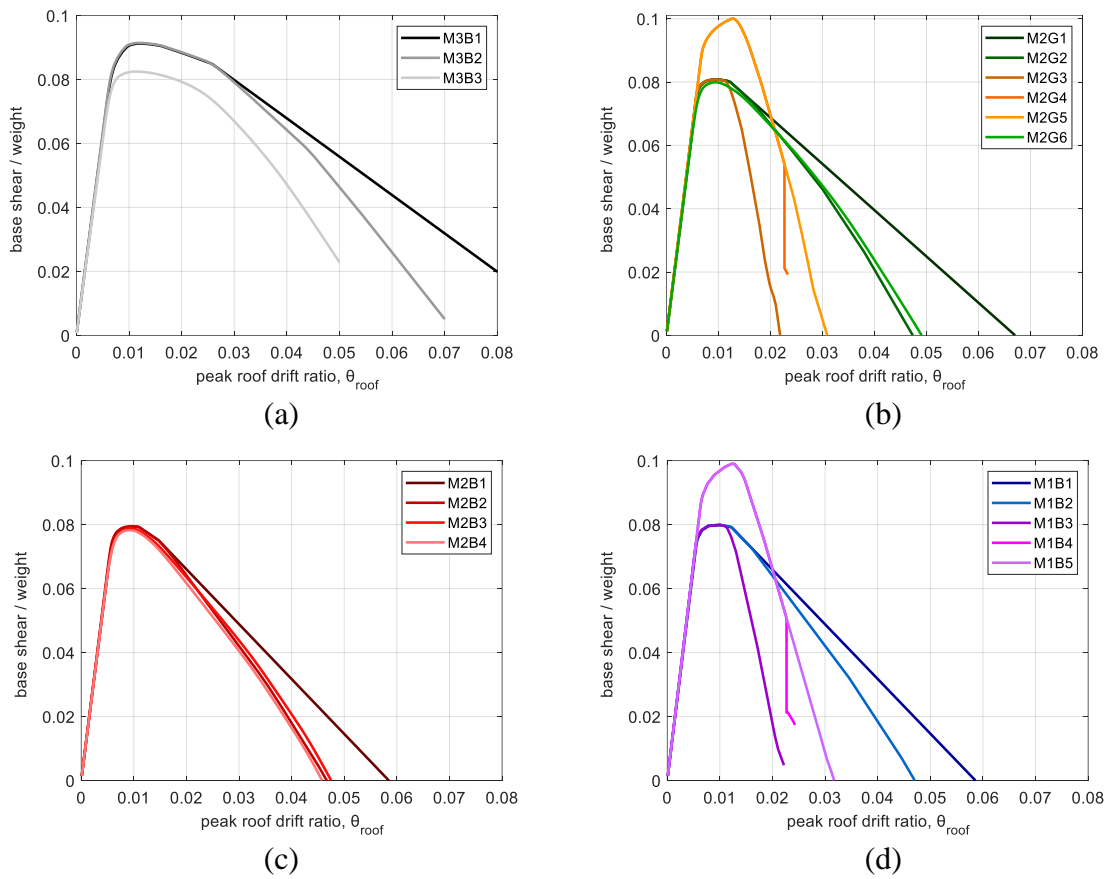
Fig. 5. Pushover Analysis results: (a) 3D with basements (M3Bx). (b) 2D no basements (M2Gx). (c) 2D with basements (M2Bx). (d) 2D one bay with basements (M1Bx).
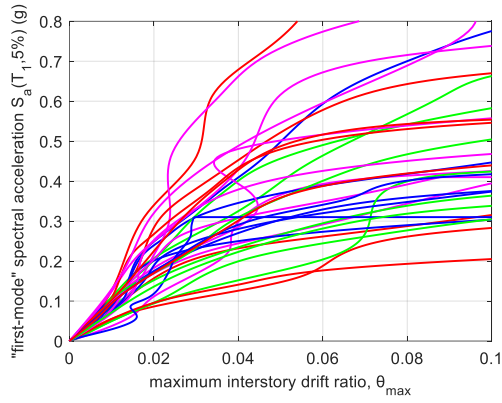
(a)
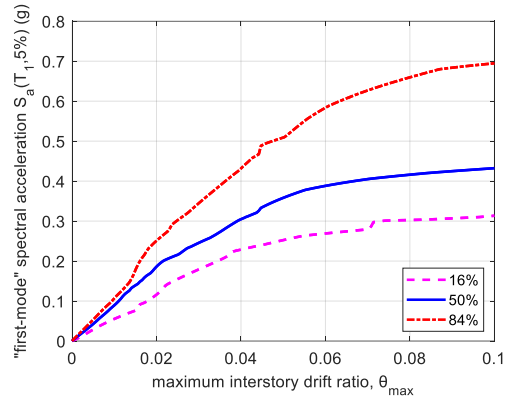
(b)

Fig. 6. Indicative results for model M3B2: (a) IDA curves, (b) 16%, 50%, 84% $S_a|\theta_{max}$ fractiles.
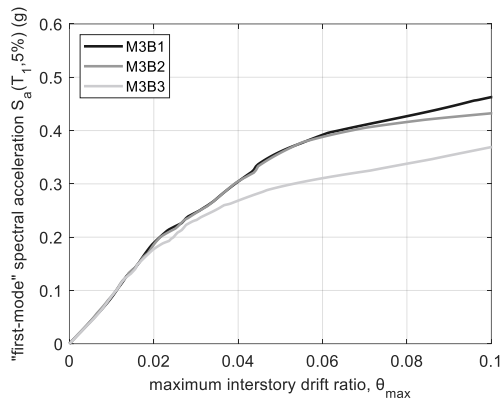
(a)
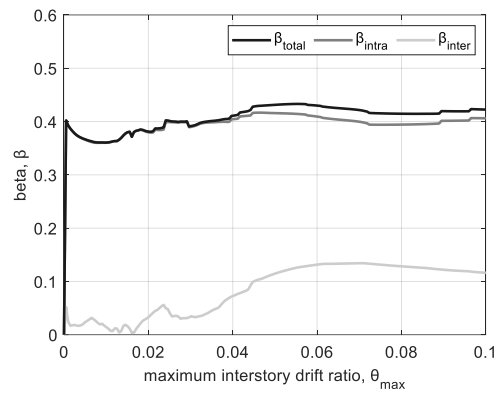
(b)
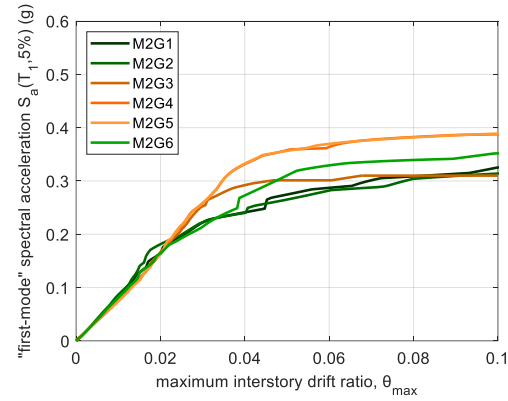
(c)
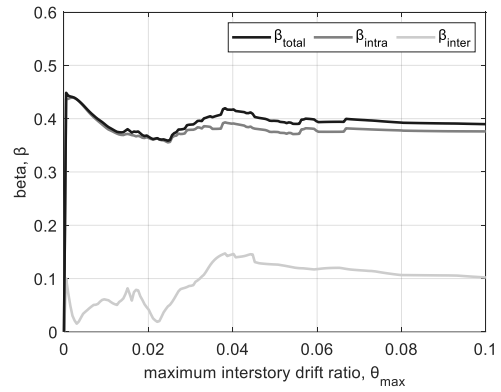
(d)
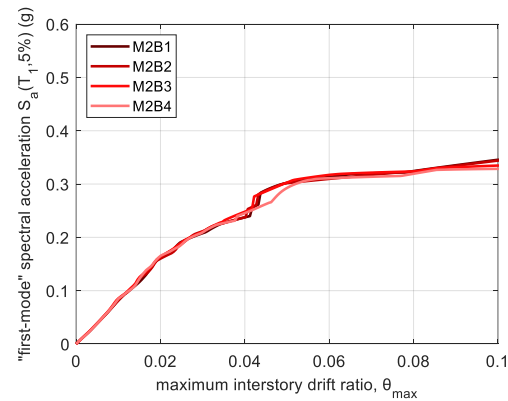
(e)
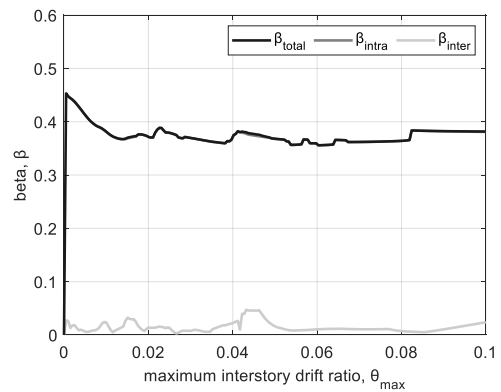
(f)
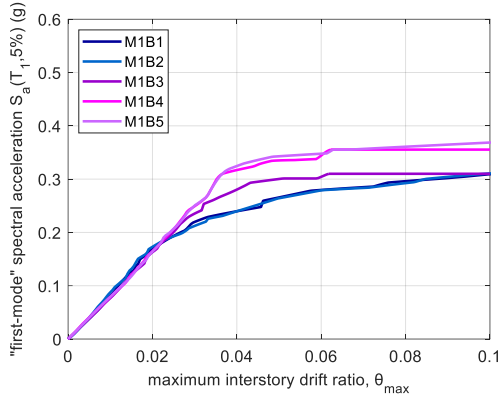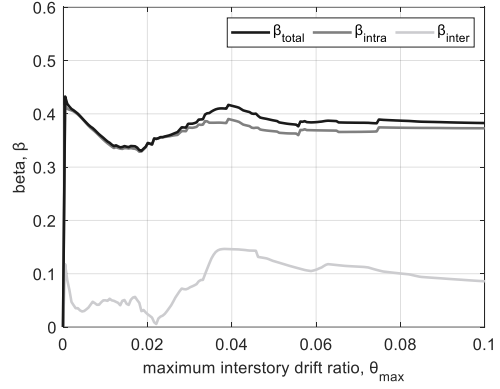
(g)   (h)

Fig. 7. MDOF median IDA curves and dispersions β_{total}, β_{intra} and β_{inter} via Eq. (11): (a) M3Bx median IDA curves. (b) M3Bx dispersions. (c) M2Gx median IDA curves. (d) M2Gx dispersions. (e) M2Bx median IDA curves. (f) M2Bx dispersions. (g) M1Bx median IDA curves. (h) M1Bx dispersions.
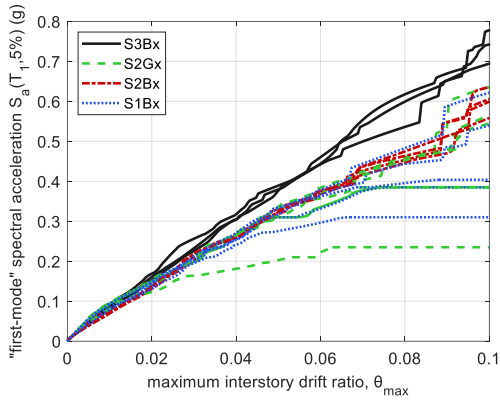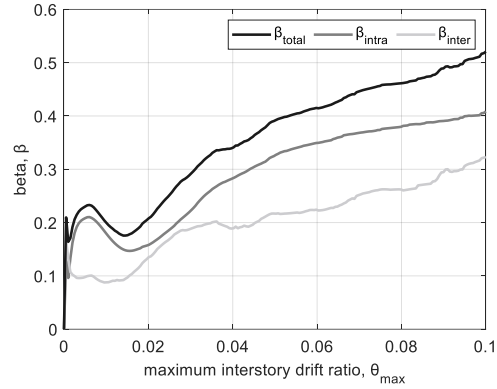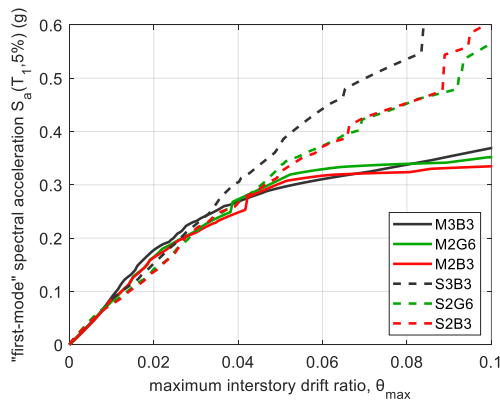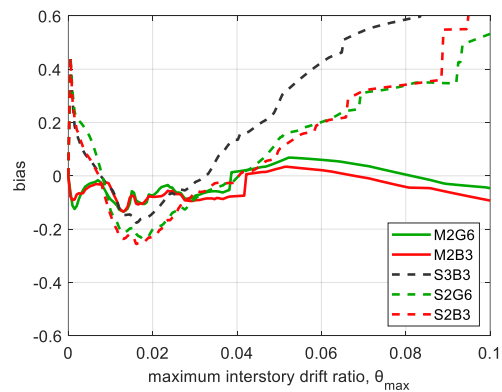

(a)   (b)

Fig. 8. SDOF median IDA curves and dispersions: β_{total}, β_{intra}, and β_{inter} via Eq. (11): (a) Sxxx median IDA curves. (b) Sxxx dispersions.

(a)   (b)

20

(c)   (d)
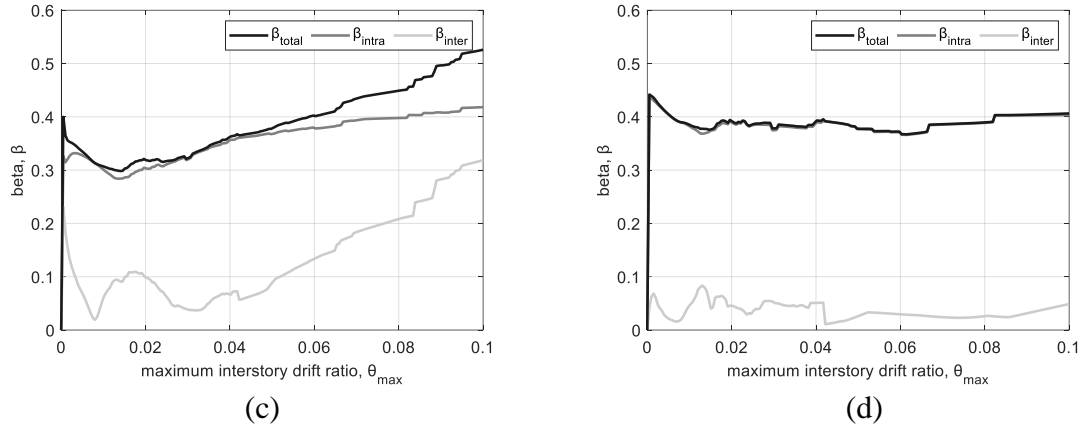
Fig. 9. Comparison between fiber models of each category: (a) Median IDA curves. (b) Relative bias (Eq. (12)) considering M3B3 as the baseline model. (c) Dispersions including the SDOFs (Eq. (11)). (d) Dispersions without the SDOFs (Eq. (11)).
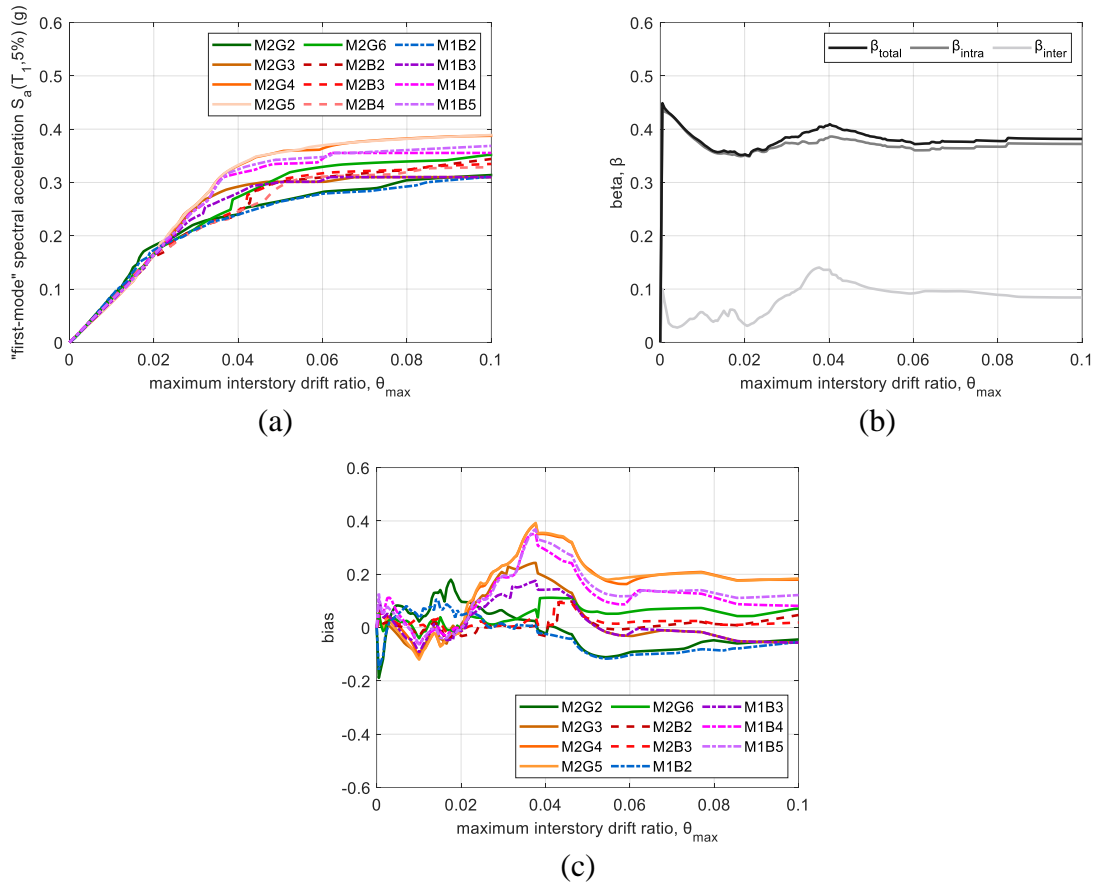

(a)   (b)

(c)

Fig. 10. Comparison between 2D models except for those where elastic elements were employed for the columns: (a) Median IDA curves. (b) Dispersions (Eq. (11)). (c) Relative bias considering M2B4 as the baseline model (Eq. (12)).
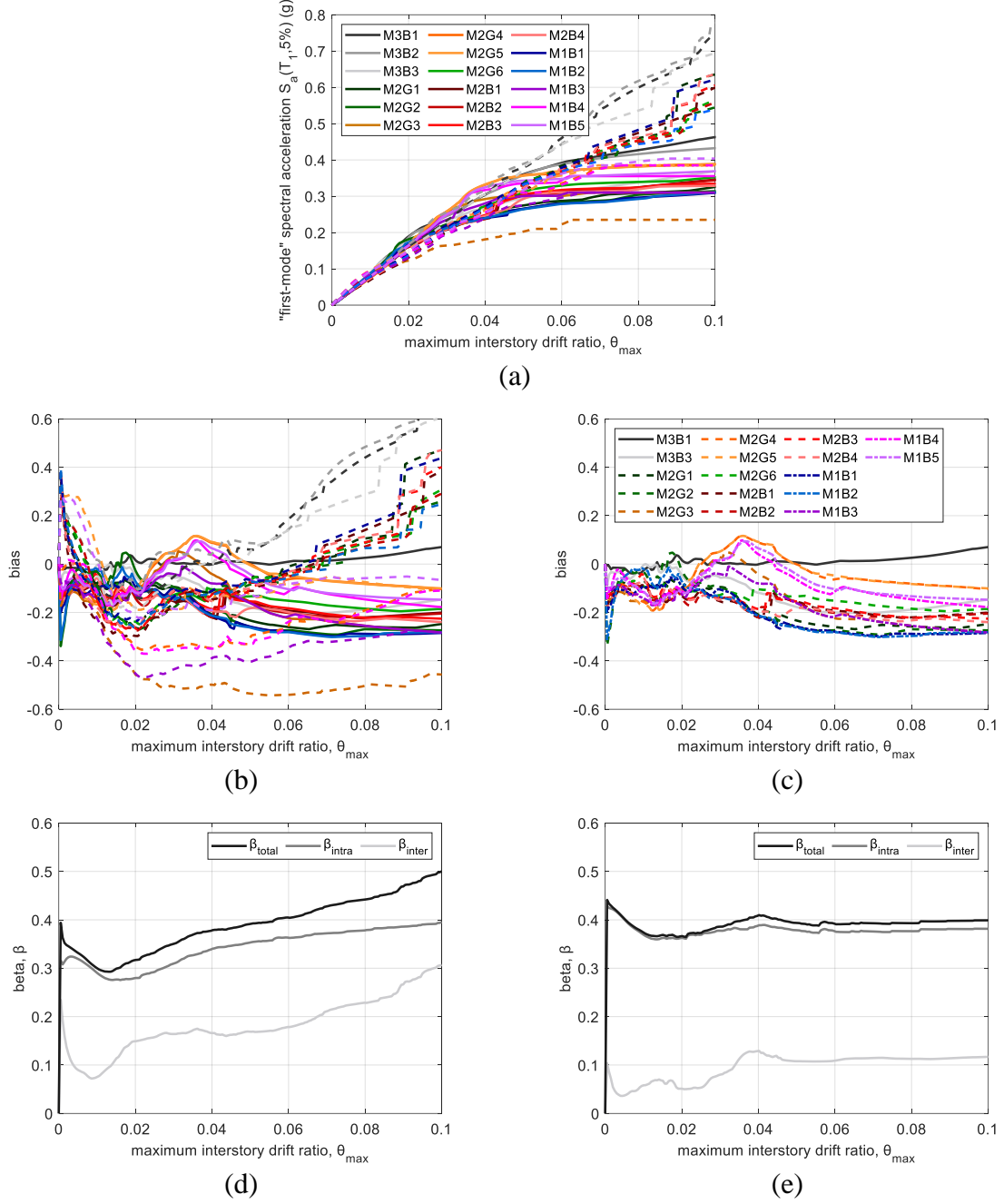
Fig. 11. Comparison between all models: (a) Median IDA curves of all models (MDOF: solid line, equivalent SDOF: dashed line). (b) Relative bias (Eq. (12)) considering M3B2 as the baseline model (MDOF: solid line, equivalent SDOF: dashed line). (c) Relative bias (Eq. (12)) considering M3B2 as the baseline model without the SDOFs. (d) Dispersions with SDOFs (Eq. (11)). (e) Dispersions without SDOFs (Eq. (11)).
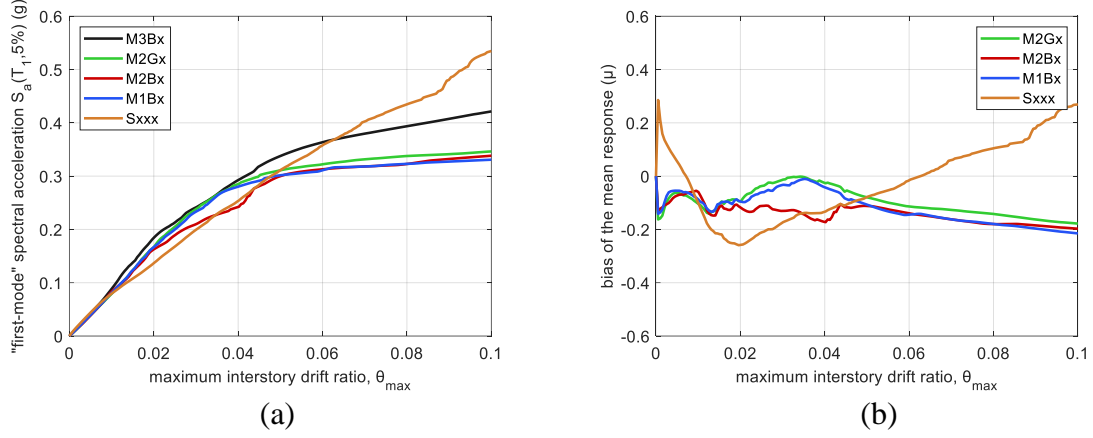
Fig. 12. (a) 50% IDA curves of the mean response μ for each model category. (b) Bias of the mean response considering M3Bx as the baseline category.
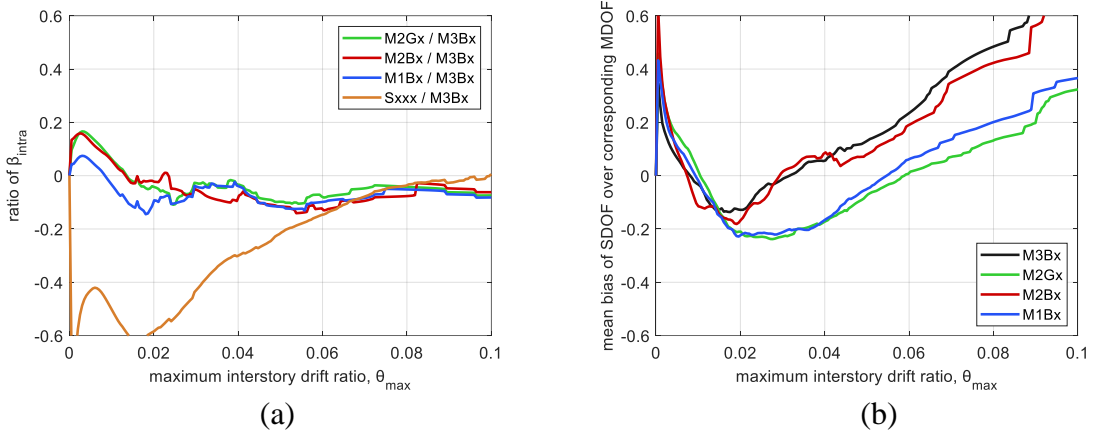

Fig. 13. (a) Ratio of mean record-to-record variability (β_{intra} Eq. (11)) between categories considering M3Bx as the baseline category. (b) Bias between mean SDOF and mean MDOF response at each category.
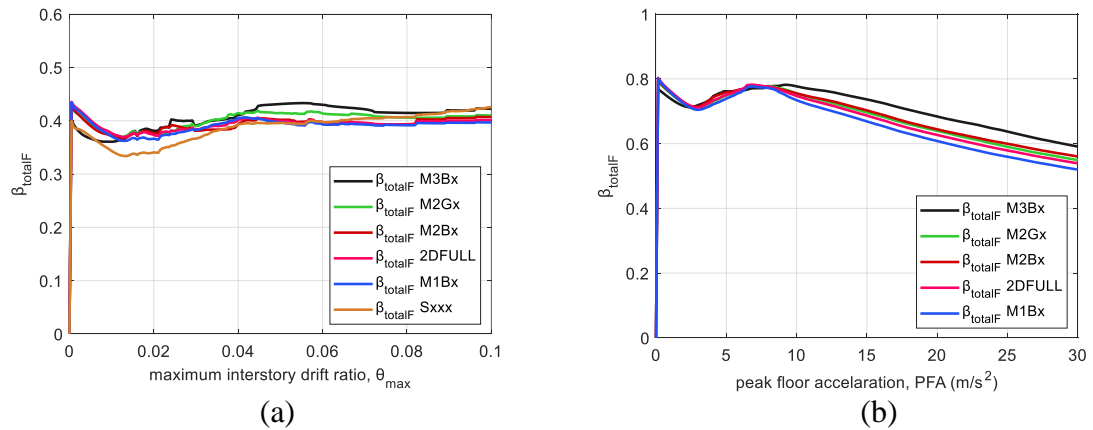

Fig. 14. Total dispersion β_{totalF} for arbitrary $S_a(T_1,5\%)$ as IM given: (a) Maximum interstory drift ratio (θ_{max}). (b) Peak floor acceleration (*PFA*).
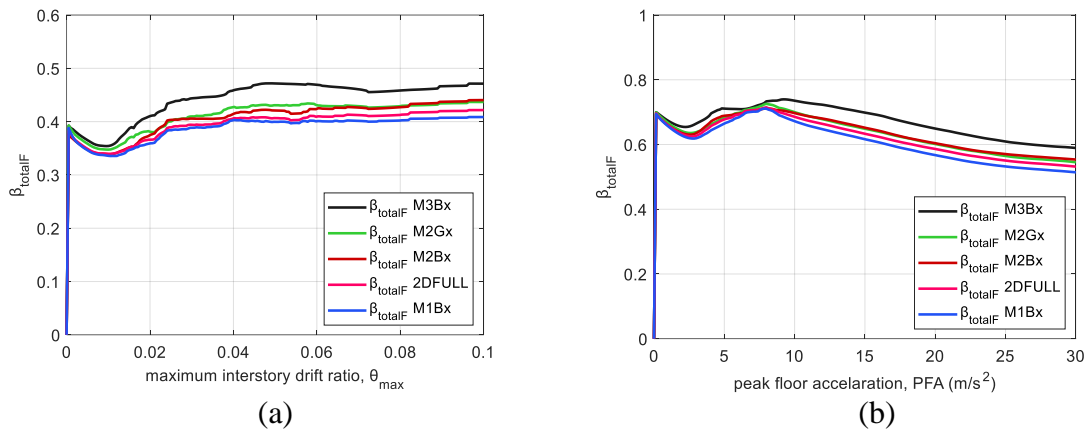
Fig. 15. Total dispersion β_{totalF} for geomean $S_{agm}(T_1, 5\%)$ as IM given: (a) Maximum interstory drift ratio (θ_{max}). (b) Peak floor acceleration (*PFA*).
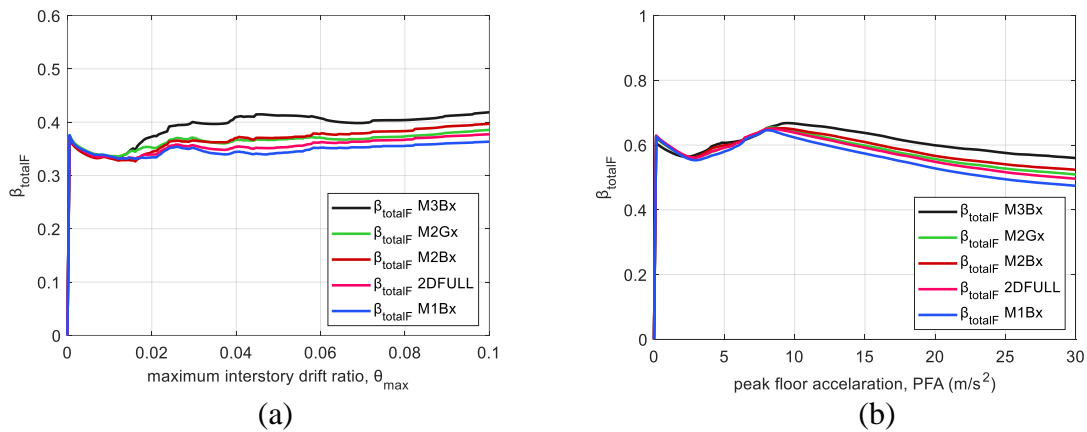

Fig. 16. Total dispersion β_{totalF} for *AvgS_a* as IM given: (a) Maximum interstory drift ratio (θ_{max}). (b) Peak floor acceleration (*PFA*).

Tables

Table 1. Overall results of the modal and the pushover analysis.

Model	T_{1x} (s)[++]	T_{1y} (s)[++]	T_{2x} (s)[++]	V_{max} (kN)	t_{po} (s)[†]	Model	T^* (s)	F^* (kN)
M3B1	3.64	3.31	1.26	9907.23	83	S3B1	3.99	7389.89
M3B2	3.61	3.29	1.25	9928.20	95	S3B2	3.90	7331.70
M3B3	3.68	3.34	1.17	8956.44	315	S3B3	3.98	6636.68
M2G1	3.81	-	1.33	8766.18[+]	30	S2G1	3.80	6405.12[+]
M2G2	3.78	-	1.32	8779.38[+]	24	S2G2	3.79	6375.08[+]
M2G3	3.78	-	1.32	8770.50[+]	9	S2G3	3.78	6365.90[+]
M2G4	3.78	-	1.32	10862.48[+]	6	S2G4	3.80	8030.36[+]
M2G5	3.78	-	1.32	10862.48[+]	6	S2G5	3.78	7928.16[+]
M2G6	3.83	-	1.33	8678.42[+]	160	S2G6	3.83	6358.92[+]
M2B1	3.84	-	1.34	8617.34[+]	35	S2B1	3.85	6322.56[+]
M2B2	3.82	-	1.33	8627.50[+]	35	S2B2	3.81	6320.04[+]
M2B3	3.86	-	1.33	8562.26[+]	129	S2B3	3.86	6311.56[+]
M2B4	3.85	-	1.33	8496.24[+]	68	S2B4	3.85	6225.26[+]
M1B1	3.78	-	1.32	8670.78[+]	11	S1B1	3.79	6285.18[+]
M1B2	3.76	-	1.32	8683.28[+]	9	S1B2	3.76	6367.44[+]
M1B3	3.76	-	1.32	8673.22[+]	6	S1B3	3.77	6350.37[+]
M1B4	3.76	-	1.32	10750.80[+]	6	S1B4	3.77	7882.97[+]
M1B5	3.76	-	1.32	10750.80[+]	6	S1B5	3.76	7883.56[+]

[+] The results from the half building multiplied by 2.

[++] T_{1x}, T_{2x} the two first vibration periods in X direction and T_{1y} the first vibration period in Y direction.

[†] Time that was required to perform pushover analysis.